

*Short Communcation*

## **Preparation of Superhydrophobic Coating on Q235 Steel and its Corrosion Resistance in Simulated Concrete Pore Solution**

Wenbiao Bai, Junyang Liu, Shuli Qi

Qingong College, North China University of Science and Technology, Tangshan 063000, China

\*E-mail: [tmgcb20@126.com](mailto:tmgcb20@126.com)

Received: 26 July 2022 / Accepted: 29 August 2022 / Published: 10 October 2022

---

Phosphate coating was prepared on the surface of Q235 steel through phosphate treatment as the bottom layer, and then the phosphate coating was uniformly covered with modified TiO<sub>2</sub> sol which was closely combined with the phosphate coating to form a superhydrophobic coating. Scanning electron microscopy, energy spectrometer, droplet contact angle meter and electrochemical workstation were used to characterize and analyze the surface morphology, composition, surface hydrophobicity and corrosion resistance of the superhydrophobic coating in simulated concrete pore solution respectively. The results show that the superhydrophobic coating has a kind of micro and nano structure, and the main composition are Zn, O, P, Ti, Si and C elements. The superhydrophobic coating is closely combined with Q235 steel to reduce the surface energy and maintain superhydrophobic state. The corrosion current density and corrosion weight gain of the superhydrophobic Q235 steel are significantly lower than that of bare Q235 steel immersed in simulated concrete pore solution for the same time. The superhydrophobic coating formed on Q235 steel can effectively inhibit the corrosion reaction with its high binding strength and good surface hydrophobic action, and shows an ideal corrosion resistance in simulated concrete pore solution.

---

**Keywords:** Superhydrophobic coating; Q235 steel; Corrosion resistance; Simulated concrete pore solution; Contact angle of water droplet

### **1. INTRODUCTION**

Q235 steel has the advantages of low cost, good plasticity, toughness, weldability and high strength, which is widely used in construction industry to meet the requirements of general steel structure and reinforced concrete structure steel [1-4]. When Q235 steel buried in the concrete environment, the alkaline environment caused by cement hydration effect and the infiltration of chloride ions will cause the damage of Q235 steel surface due to corrosion. Therefore, the phenomenon of steel corrosion in concrete is common. Researchers have been committed to studying

the corrosion behavior of steel in concrete environment, and exploring ways to improve the corrosion resistance of steel in concrete environment [5-9].

Research shows that surface treatment is an easy and effective way to improve the corrosion resistance of steel. Using the surface treatment methods to form a protective coating covered on the steel surface can effectively block the corrosion medium, so as to slow down the corrosion rate [10-14]. Moreover, if a protective coating with hydrophobic or superhydrophobic property is formed through surface treatment, it is expected to further improve the corrosion resistance [15-18]. Therefore, in the paper, a zinc phosphate coating was prepared on the surface of Q235 steel through phosphate treatment as the bottom layer, and then the phosphate coating was uniformly coated with modified TiO<sub>2</sub> sol which was closely combined with the phosphate coating to form a superhydrophobic coating. The surface morphology, composition and stability of the superhydrophobic coating were characterized, and then the corrosion protection of the superhydrophobic coating on Q235 steel in simulated concrete pore solution was further studied.

## 2. EXPERIMENTAL

### 2.1 Materials and chemical agents

A Q235 cold-rolled steel plate was cut into numerous rectangular samples of 5 cm×3 cm×2 cm as the experimental substrate. The chemical agents used in the pretreatment of samples and experimental stage mainly include: sodium hydroxide, sodium carbonate, sodium phosphate, sodium bicarbonate, hydrochloric acid, absolute ethanol, zinc oxide, phosphoric acid, nitric acid, phytic acid, nickel nitrate, deionized water, etc.

### 2.2 Preparation of superhydrophobic coating on Q235 steel

A superhydrophobic coating was prepared on the surface of Q235 steel sample, and the specific steps were as follows:

Step 1: Remove the oil on the surface of Q235 steel sample by immersing in 70°C alkaline solution (sodium hydroxide 35 g/L + sodium carbonate 10 g/L + sodium phosphate 6 g/L) for 10 minutes, and then activate it in hydrochloric acid with 15% volume fraction for 1 minute.

Step 2: Place the pretreated Q235 steel sample in 50°C phosphate solution (zinc oxide 30 g/L + phosphoric acid 22 g/L + nitric acid 6 g/L + phytic acid 1 g/L + nickel nitrate 1 g/L) for 20 minutes. During phosphate process, the surface of Q235 steel is dissolved in the phosphate solution to form phosphate precipitate, resulting in multiple chemical and electrochemical reactions. Phosphate precipitates together with water molecules to form crystal nuclei, which gradually grow into grains, and many grains were tightly packed on the surface of Q235 steel to form a phosphate coating.

Step 3: Take 500 mL of TiO<sub>2</sub> sol (containing nano-TiO<sub>2</sub> particles with mass fraction of about 30%), and slowly add 5 g of hexadecyltrimethoxysilane. During the stirring process, the hydrolysis and condensation reaction of hexadecyltrimethoxysilane occurred to generate a hydrophobic group, which was branched to the hydroxyl group of TiO<sub>2</sub> particles to achieve surface modification, thus obtaining a modified TiO<sub>2</sub> sol. After standing for 24 h, the modified sol was uniformly coated on the surface of the samples after phosphate treatment, and then the sample was put into a thermostatic drying box at the temperature of 200 °C for 1 h. During the heating process, the modified sol was closely combined with phosphate coating, and a superhydrophobic coating was successfully prepared on the surface of Q235 steel sample. In the following description below, the untreated sample was named bare Q235 steel, and the sample coated with a superhydrophobic coating was named superhydrophobic Q235 steel.

### 2.3 Characterization and Performance Testing

#### 2.3.1 Surface morphology and composition analysis

The samples were sprayed with gold by ion sputtering apparatus to improve surface conductivity. And then, the sprayed samples were placed on the workbench of scanning electron microscope. The surface morphology of bare Q235 steel and superhydrophobic Q235 steel were characterized under 10000 times magnification. At the same time, the composition of bare Q235 steel and superhydrophobic Q235 steel were analyzed by X-MAX 80 energy dispersive spectrometer (EDS).

#### 2.3.2 Surface hydrophobicity and stability testing

OCA15Pro contact angle measuring instrument was used for measuring the contact angle of water droplets dropped at five different positions on the surface of samples. The volume of each water droplet was 5 µL, and the hydrophobicity of the samples surface was evaluated according to the measurement results. When the contact angle of water droplet exceeds 90°, the sample shows hydrophobicity. Especially when the contact angle of water droplet exceeds 150°, the sample shows superhydrophobicity.

Schematic diagram of the experimental device as shown in Figure 1 was used for testing the surface stability of superhydrophobic Q235 steel by sand-falling impact. A certain amount of sand particles with uniform particle size (about 200 µm) were dropped vertically along the conduit of funnel to do impact on the sample surface with a tendency of 45°. The experiment was repeated for five times. The contact angle of water droplet was measured at the end of each experiment, and the surface stability of superhydrophobic Q235 steel was evaluated according to the measurement results.

Schematic diagram of the experimental device shown in Figure 2 was used for further testing the surface stability of superhydrophobic Q235 steel by ultrasonic oscillation. The sample was placed vertically and immersed in anhydrous ethanol, and ultrasonic wave of 40 kHz and 120 W were generated by an ultrasonic generator, which oscillated successively for 40 s, 80 s, 120 s, 180 s and 240 s. The contact angle of water droplet was measured at the end of each experiment, and the surface stability of superhydrophobic Q235 steel was further evaluated according to the measurement results.

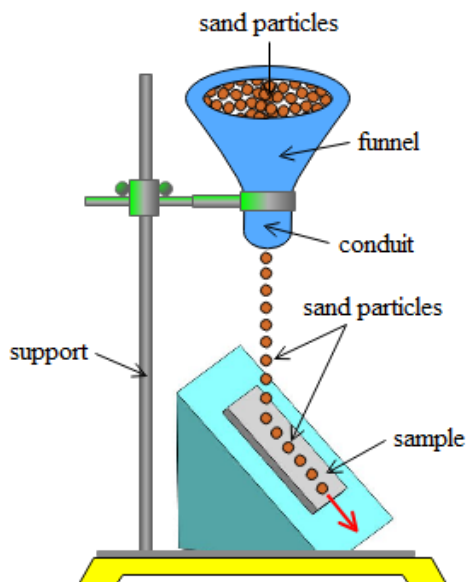


**Figure 1.** Schematic diagram of sand-falling impact experimental device

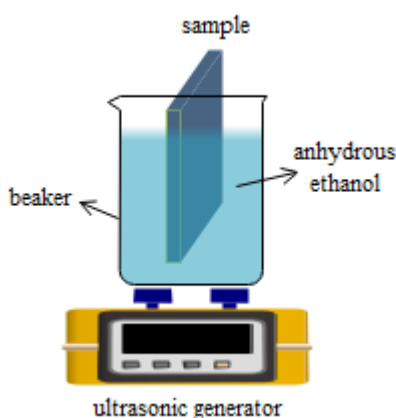


**Figure 2.** Schematic diagram of ultrasonic oscillation experimental device

### 2.3.3 Corrosion resistance testing

Saturated calcium hydroxide solution was selected as the main composition of simulated concrete pore solution and 0.8 mol/L sodium bicarbonate was added to adjust the pH value of the solution to about 12.0. After that, 0.5 mol/L sodium chloride was added to prepare the simulated concrete pore solution. Parstat 2273 electrochemical workstation was used for testing the corrosion resistance of bare Q235 steel and superhydrophobic Q235 steel. Different samples was the working electrode, and the saturated calomel electrode and the platinum electrode were the reference electrode and the counter electrode, respectively. The polarization curves of different samples after immersion in simulated concrete pore solution for different time were tested. The scanning rate of the polarization curve was 1 mV/s, and the test results were imported into the PowerSuite software and fitted by Tafel extrapolation to obtain the corrosion potential and corrosion current density. In addition, the corrosion weight gain of different samples after immersion in simulated concrete pore solution for different time

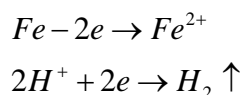
were also calculated which provides a basis for further evaluating the corrosion resistance of superhydrophobic Q235 steel.

### 3. RESULTS AND DISCUSSIONS

#### 3.1 Surface morphology and composition

As shown in Figure 3(a), many scratches and minor defects exist on the surface of bare Q235 steel, which are the traces left by the pretreatment stage. As shown in Figure 3(b), a phosphate coating with flake-like grains is formed on the surface of Q235 steel after phosphate treatment, showing uneven and rough features with some pores. The phosphate treatment can be considered as the dissolution of Q235 steel immersed in phosphate solution and the combination of phosphate and metal ions to form phosphate precipitate, resulting in multiple chemical and electrochemical reactions listed in equation (1)~(3). Phosphate precipitates together with water molecules to form crystal nuclei, which gradually grow into grains, and many grains are tightly packed on the surface of Q235 steel to form a phosphate coating [19-21].

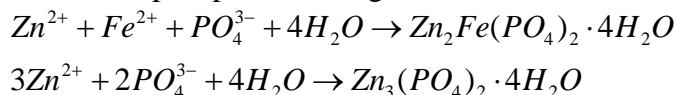
(1) dissolution of Q235 steel:



(2) dissociation of phosphoric acid:



(3) phosphate precipitation and phosphate coating formation:



As shown in Figure 3(c), a special coating with micro and nano structure completely covers Q235 steel surface, mainly composed of cluster bumps or pores. This special structure is formed after phosphate treatment and modified TiO<sub>2</sub> sol treatment, which can give Q235 steel some excellent physical and chemical properties, such as superhydrophobic property.

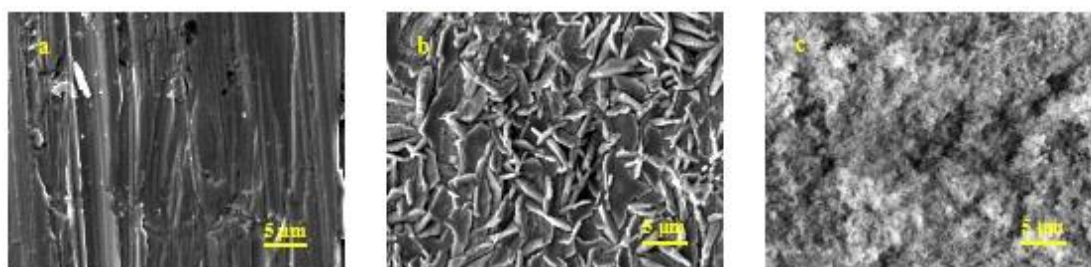


**Figure 3.** Surface morphology of different samples: a-bare Q235 steel; b-Q235 steel after phosphate treatment; c-superhydrophobic Q235 steel

Figure 4(a) shows the EDS spectrum and analysis results of bare Q235 steel, Figure 4(b) shows the EDS spectrum and analysis results of Q235 steel after phosphate treatment and Figure 4(c) shows the EDS spectrum and analysis results of superhydrophobic Q235 steel. Combined with Figure 4(a), Figure 4(b) and Figure 4(c), it can be seen that the main composition of phosphate coating formed on Q235 steel are Zn, O and P elements. However, the main composition of the superhydrophobic coating formed on Q235 steel by phosphate treatment and then coating modified sol are Zn, O, P, Ti, Si and C elements, of which Ti, Si and C elements are derived from the modified sol.

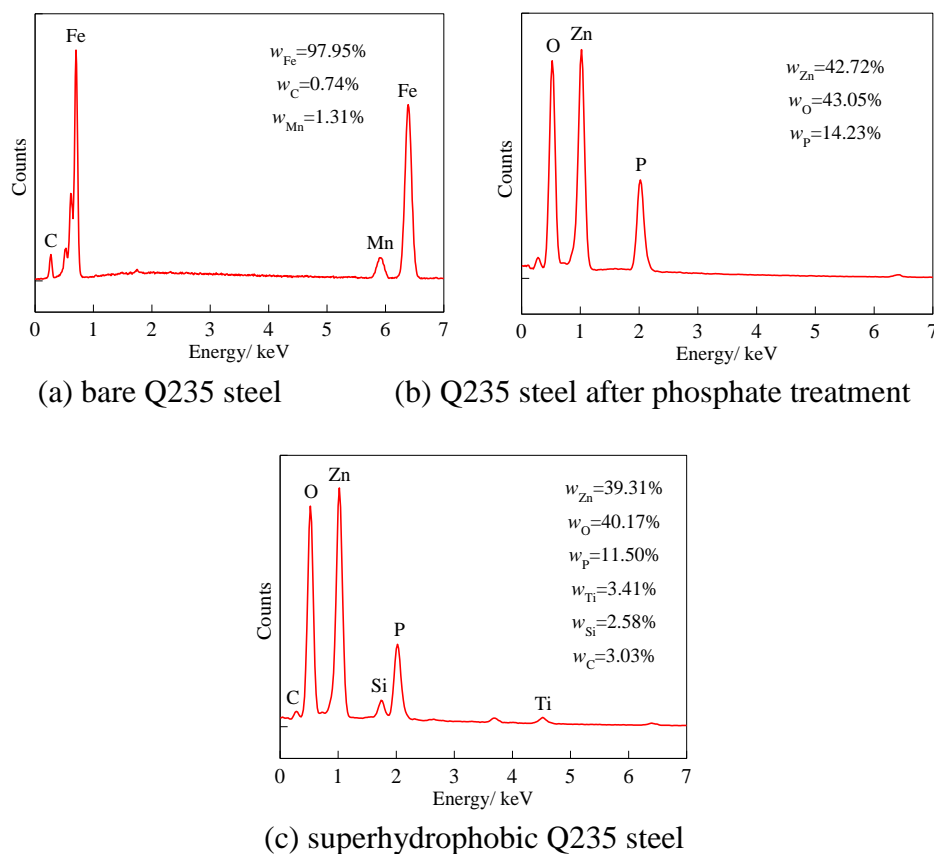
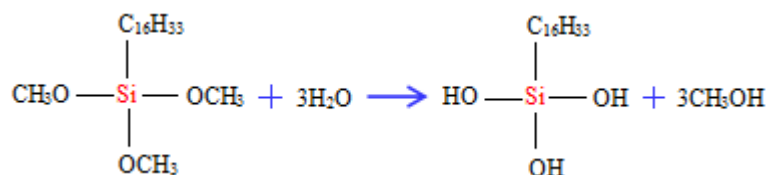


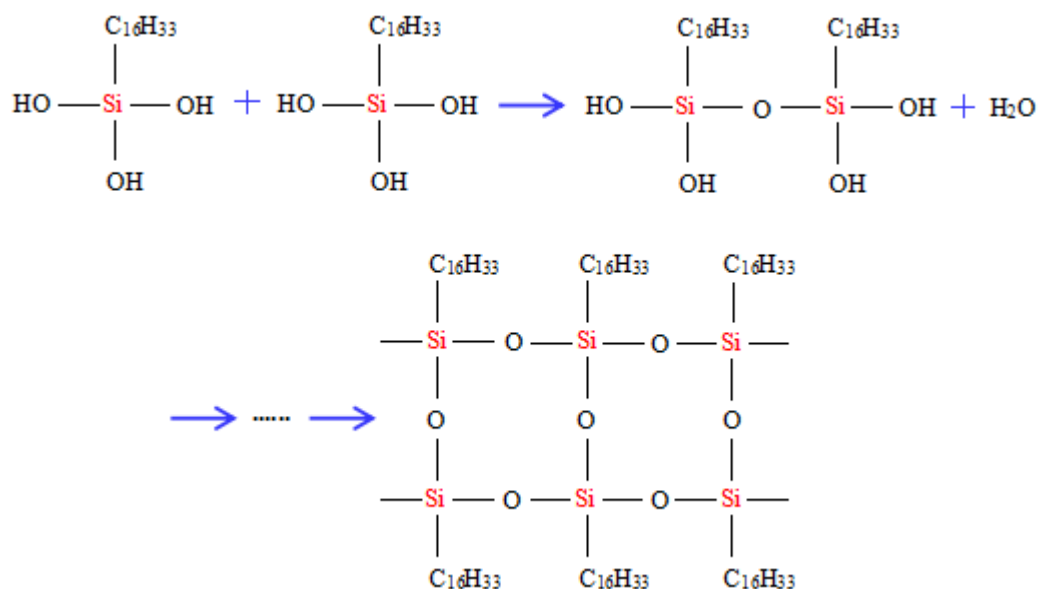
**Figure 4.** EDS spectrum and analysis results of different samples

The surface modification mechanism and method of  $TiO_2$  particles using hexadecyltrimethoxysilane is listed in equation (4) and (5) which is also reported in many papers [22-25]. During the stirring process, hexadecyltrimethoxysilane successively undergoes hydrolysis reaction, dehydration condensation reaction to generate a hydrophobic group containing Si element, which are attached to the hydroxyl group of  $TiO_2$  particles to realize surface modification of  $TiO_2$  particles. The sol containing modified  $TiO_2$  particles is uniformly coated on the surface of Q235 steel after phosphate treatment, which further promote hydrolysis reaction and dehydration condensation reaction in the heating process. After heating the modified sol, the sol is closely combined with the phosphate coating to form a superhydrophobic coating, thus introducing Ti, Si and C elements.

(4) hydrolysis reaction:

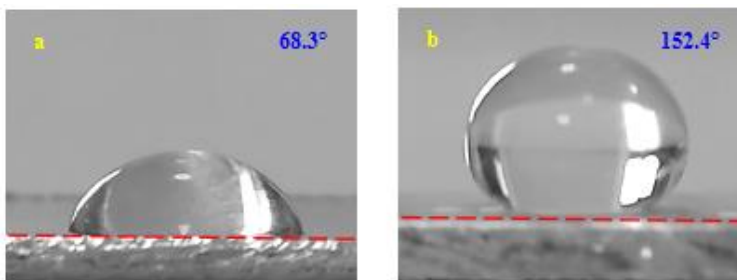


(5) dehydration condensation reaction:



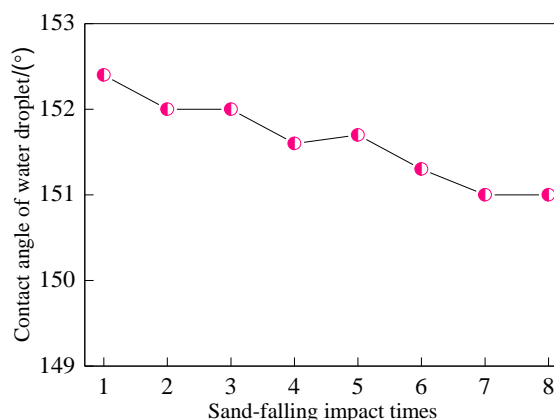
### 3.2 Surface hydrophobicity and stability analysis

Figure 5(a) shows the surface morphology and contact angle of water droplet on bare Q235 steel surface, and Figure 5(b) shows the surface morphology and contact angle of water droplet on superhydrophobic Q235 steel surface. Combined with Figure 5(a) and Figure 5(b), it is clear that through phosphate treatment and then coating modified  $\text{TiO}_2$  sol make Q235 steel surface appear superhydrophobicity, and the contact angle of water droplet reaches  $152.4^\circ$ . Many researchers verify that the  $\text{TiO}_2$  has better superhydrophobicity performance published in many literatures [26-28]. The reason is that in the process of preparing modified sol, the hydrolysis and condensation reaction of hexadecyltrimethoxysilane forms a hydrophoxy group grafted to  $\text{TiO}_2$  particles to achieve surface modification, so that  $\text{TiO}_2$  particles have low surface energy. After curing, a coating is formed and closely combined with the phosphate coating to form a superhydrophobic coating with a micro and nano structure. The superhydrophobic coating has a weak affinity with water, which makes it difficult for water droplets to spread on the surface, thus showing superhydrophobicity [29-30].



**Figure 5.** Surface morphology and contact angle of water droplet on surface of different samples: a- bare Q235 steel; b-superhydrophobic Q235 steel

Figure 6 shows the variation trend of the contact angle of water droplet on superhydrophobic Q235 steel surface with the increase of sand-falling impact times. Figure 7 shows the variation trend of the contact angle of water droplet on superhydrophobic Q235 steel surface with the extension of ultrasonic oscillation time. It can be seen from Figure 6 that the contact angle of water droplets still exceeds  $150^\circ$  after 8 times of sand-falling impact, indicating that the superhydrophobic coating has high bond strength with Q235 steel and can maintain the superhydrophobic state stably. As can be seen from Figure 7, with the prolongation of ultrasonic oscillation time, the droplet contact angle fluctuates, but the variation range is very small. The contact angle of water droplets still exceeds  $150^\circ$  after 240 s of ultrasonic oscillation, which further confirms that the superhydrophobic coating is closely bonded to Q235 steel and can keep the superhydrophobic state stably.



**Figure 6.** Variation trend of contact angle of water droplet on superhydrophobic Q235 steel with increasing of sand-falling impact times

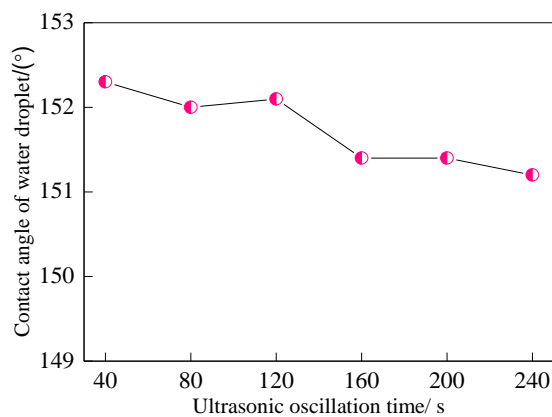


**Figure 7.** Variation trend of contact angle of water droplet on superhydrophobic Q235 steel with prolongation of ultrasonic oscillation time

### 3.3 Corrosion resistance analysis

#### 3.3.1 Polarization curves

Figure 8 shows the polarization curves of bare Q235 steel and superhydrophobic Q235 steel after immersion in simulated concrete pore solution for different time. Table 1 lists the variation trend of corrosion potential and corrosion current density of bare Q235 steel and superhydrophobic Q235 steel. Combining with Figure 8 and Table 1, it can be seen that with the prolongation of immersion time, the corrosion potential of bare Q235 steel and superhydrophobic Q235 steel moves towards the negative direction, accompanied by the increase of corrosion current density. The corrosion current density of bare Q235 steel increases significantly from  $5.28 \times 10^{-5} \text{ A/cm}^2$  to  $3.19 \times 10^{-4} \text{ A/cm}^2$ , while the corrosion current density of superhydrophobic Q235 steel increases from  $2.71 \times 10^{-6} \text{ A/cm}^2$  to  $7.22 \times 10^{-6} \text{ A/cm}^2$ . However, the change amplitude of corrosion potential is small, because the corrosion potential is mainly related to the composition of materials. Although corrosion will lead to the formation of new products and cover the surface of bare Q235 steel and superhydrophobic Q235 steel, the content of corrosion products is similar to that of Q235 steel. The proportion of the ratio is low, so the corrosion potential changes less.

Compared with bare Q235 steel, the change amplitude of corrosion current density of superhydrophobic Q235 steel is obviously smaller. The reason is that the superhydrophobic Q235 steel surface has a micro and nano structure that can intercept air. When the sample immersed in simulated concrete pore solution, the intercepted air on the surface of superhydrophobic Q235 steel can play a physical barrier to block corrosive ions, making it difficult to contact with Q235 steel, and effectively inhibit the corrosion reaction [31-33]. Therefore, superhydrophobic Q235 steel shows ideal corrosion resistance in simulated concrete pore solution due to the  $\text{TiO}_2$  particles. It is reported that the  $\text{TiO}_2$  has optimal corrosion resistance [34-35]. However, the corrosion current density of bare Q235 steel increases continuously after immersion in simulated concrete pore solution for more than 144 h, while that of superhydrophobic Q235 steel tends to be constant. The results show that the corrosion degree of bare Q235 steel is further aggravated in this stage, while that of superhydrophobic Q235 steel is not

aggravated, which confirms the ideal durability of superhydrophobic Q235 steel in simulated concrete pore solution.

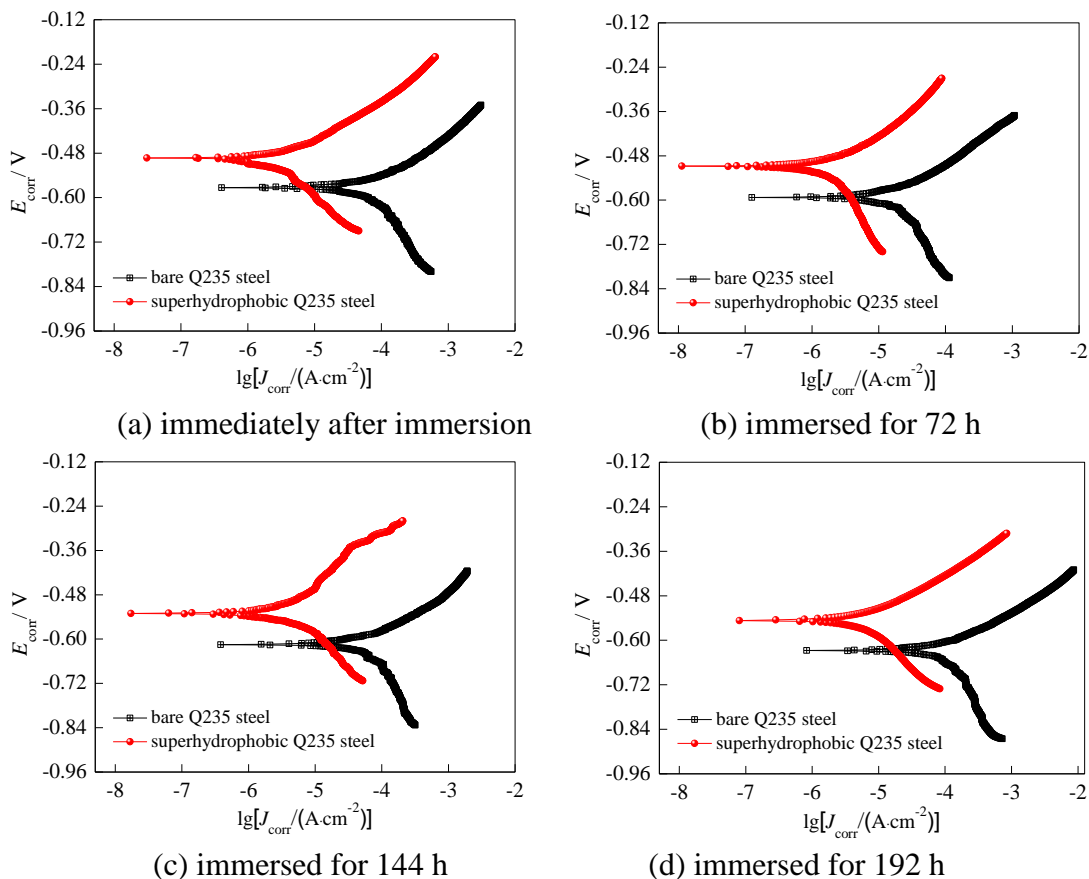


**Figure 8.** Polarization curves of bare Q235 steel and superhydrophobic Q235 steel after immersion in simulated concrete pore solution for different time

**Table 1.** Change trend of corrosion potential and current density of bare Q235 steel and superhydrophobic Q235 steel

Different samples	Corrosion potential/ V				Corrosion current density/ (A·cm <sup>-2</sup> )			
	immediately after immersion	immersed for 72 h	immersed for 144 h	immersed for 192 h	immediately after immersion	immersed for 72 h	immersed for 144 h	immersed for 192 h
bare Q235 steel	-0.573	-0.592	-0.613	-0.627	5.28×10 <sup>-5</sup>	7.59×10 <sup>-5</sup>	1.32×10 <sup>-4</sup>	3.19×10 <sup>-4</sup>
superhydrophobic Q235 steel	-0.494	-0.508	-0.530	-0.545	2.71×10 <sup>-6</sup>	3.98×10 <sup>-6</sup>	7.72×10 <sup>-6</sup>	8.01×10 <sup>-6</sup>

### 3.3.2 Corrosion weight gain

Figure 9 shows the variation trend of corrosion weight gain of bare Q235 steel and superhydrophobic Q235 steel after immersion in simulated concrete pore solution. It can be seen from Figure 9 that with the prolongation of immersion time to 192 h, the corrosion weight gain of bare Q235 steel shows a significant increasing trend, while the corrosion weight gain of superhydrophobic Q235

steel first increases and then tends to be basically constant. The reason is that the superhydrophobic Q235 steel effectively blocks the contact of corrosive ions with its surface for a period of time by virtue of its strong superhydrophobic effect, and reduces the corrosion degree. Therefore, the corrosion weight gain of the superhydrophobic Q235 steel in simulated concrete pore solution is significantly lower than that of bare Q235 steel. With the prolongation of immersion time, a loose corrosion products coating forms on the surface of bare Q235 steel, which induces further penetration of the corrosive medium, resulting in aggravation of the corrosion degree and the increase of corrosion weight gain. However, a relatively stable and dense corrosion products coating forms on the surface of superhydrophobic Q235 steel, which prevents further penetration of the corrosive medium, so its corrosion degree is not aggravated, and its durability in simulated concrete pore solution is ideal. The relationship between superhydrophobic performance and corrosion resistance is investigated in many literatures [36-37].

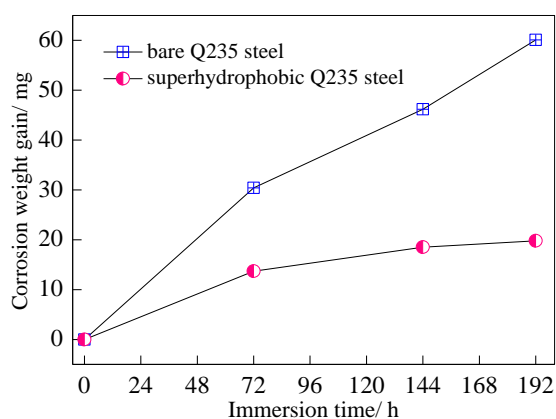


**Figure 9.** Variation trend of corrosion weight gain of bare Q235 steel and superhydrophobic Q235 steel after immersion in simulated concrete pore solution for different time

#### 4. CONCLUSIONS

(1) A superhydrophobic coating was successfully prepared on the surface of Q235 steel through phosphate treatment combined with sol-gel method. The main composition of superhydrophobic coating are Zn, O, P, Ti, Si and C elements, which could stably maintain superhydrophobic state. The corrosion current density and corrosion weight gain of superhydrophobic Q235 steel are obviously lower than those of bare Q235 steel when immersed in simulated concrete pore solution for the same time. With the prolongation of immersion time to 192 h, the corrosion current density and corrosion weight gain of superhydrophobic Q235 steel increase firstly and then tends to be basically constant.

(2) The superhydrophobic coating with micro and nano structure mainly composed of cluster bumps or pores, and the modified  $\text{TiO}_2$  sol makes it has low surface energy and weak affinity with water. The superhydrophobic coating can effectively inhibit corrosion reaction and prevent the penetration of corrosive media by virtue of its high binding strength and strong surface hydrophobicity.

Therefore, the superhydrophobic Q235 steel shows ideal corrosion resistance in simulated concrete pore solution.

#### ACKNOWLEDGEMENTS

This paper is supported by the higher education teaching reform research and practice project of Hebei Provincial Department of Education (2021GJJG619).

#### References

1. J. Z. Hu, S. M. Wang, X. L. Zhao, S. L. Zhu and B. T. Yu, *Front. Chem. Eng. China*, 5 (2010) 189.
2. Y. Zhang, Y. D. Gao, J. P. Zhou, D. Q. Sun and H. M. Li, *Met. Mater. Int.*, 27 (2021) 1224.
3. Y. Liu, X. X. Guo, B. Z. Wang, P. X. Gong, Y. P. Liu, H. J. Li and Y. C. Wu, *J. Mol. Liq.*, 360 (2022) 119513.
4. X. W. Huang, Y. L. Yuan, J. Zhao and C. C. Wei, *J. Constr. Steel Res.*, 194 (2022) 107308.
5. J. Li, H. Su, F. Chai, X. P. Chen, X. Y. Li and H. M. Meng, *J. Iron. Steel Res. Int.*, 22 (2015) 352.
6. W. Wei, X. Q. Wu, W. Ke, S. Xu, B. Feng and B. T. Hu, *J. Mater. Eng. Perform.*, 26 (2017) 4340.
7. Y. J. Li, J. J. Wu, D. Zhang, Y. Wang and B. R. Hou, *J. Solid State Electrochem.*, 14 (2010) 1667.
8. Y. Z. Zhao, T. Pan, X. T. Yu and D. Chen, *Corros. Sci.*, 158 (2019) 108097.
9. X. P. Wang, M. H. Shao, C. Q. Ye, S. G. Dong, R. G. Du and C. J. Lin, *J. Electroanal. Chem.*, 895 (2021) 115454.
10. S. H. Hu, M. Muhammad, M. Wang, R. N. Ma, A. Du, Y. Z. Fan, X. M. Cao and X. Zhao, *Mater. Lett.*, 265 (2020) 127256.
11. M. Tabish, J. M. Zhao, A. Kumar, J. T. Yan, J. B. Wang, F. Shi, J. Zhang, L. J. Peng, M. A. Mushtaq and G. Yasin, *Chem. Eng. J.*, 450 (2022) 137624.
12. S. H. Dong, Y. Yang, T. T. Liang, R. N. Ma, A. Du, M. X. Yang, Y. Z. Fan, X. Zhao and X. M. Cao, *Surf. Coat. Technol.*, 422 (2021) 127551.
13. Y. Wu, Y. Y. Duan, J. Qiu, X. Gao and H. Y. Ma, *Appl. Surf. Sci.*, 578 (2022) 151980.
14. L. H. Guo, Q. Huang, C. Zhang, J. Wang, G. P. Shen, C. L. Ban and L. X. Guo, *Corros. Sci.*, 178 (2021) 108960.
15. G. W. Wang, J. H. Jiang, Y. X. Qiao, L. Gu, E. E. Klu, X. Y. Gong, A. Ma and D. Song, *J. Alloys Compd.*, 921 (2022) 166044.
16. M. Tabish, M. U. Malik, M. A. Khan, M. J. Anjum, N. Muhammad, A. Ahmad, S. Ibraheem, A. Kumar, T. A. Nguyen and G. Yasin, *Thin Solid Films*, 756 (2022) 139373.
17. W. T. Liu, Z. L. Mo, C. Shuai, S. He, R. M. Yue, X. D. Guo, Y. Chen, H. Zheng, J. C. Zhu, R. B. Guo and N. J. Liu, *Colloids Surf., A*, 467 (2022) 129056.
18. S. H. Lei, S. Wang, H. Zhong, Z. F. Cao and X. P. Huang, *Colloids Surf., A*, 626 (2021) 127015.
19. Y. W. Song, D. Y. Shan, R. S. Chen, F. Zhang and E. H. Han, *Corros. Sci.*, 51 (2009) 62.
20. C. Kabitha, T. S. N. Narayanan, K. Ravichandran, I. S. Park and M. H. Lee, *J. Coat. Technol. Res.*, 11 (2014) 431.
21. L. Kouisni, M. Azzi, M. Zertoubi, F. Dalard and S. Maximovitch, *Surf. Coat. Technol.*, 185 (2004) 58.
22. J. Alvarado, G. Acosta and F. Perez, *Polym. Degrad. Stab.*, 134 (2016) 376.
23. A. Jahell, A. Guillermo and P. Fatima, *Data Brief*, 16 (2018) 1038.
24. S. Mugundan, P. Praveen, S. Sridhar, S. Prabu, K. L. Mary, M. Ubaidullah, S. F. Shaikh and S. Kanagesan, *Inorg. Chem. Commun.*, 139 (2022) 109340.

25. K. P. Devi, P. Goswami and H. Chaturvedi, *Appl. Surf. Sci.*, 591 (2022) 153226.
26. C. B. Hu, K. Kwan, X. Y. Xie, C. G. Zhou and K. N. Ren, *React. Funct. Polym.*, 23 (2022) 105381.
27. H. Li, J. Lai, M. Yao, Y. M. Leng, Z. D. Wu, J. Zhang, H. L. Peng and Z. M. Qiu, *Appl. Surf. Sci.*, 601 (2022) 154109.
28. Y. X. Xiang, Y. He, W. W. Tang, H. J. Li, Y. H. Zhang, R. X. Song, B. Liu, Y. H. He, X. Guo and Z. He, *Colloids Surf., A*, 629 (2021) 127394.
29. S. Ibrahim and M. Sultan, *Silicon Chem.*, 12 (2020) 805.
30. J. G. Fu, Y. H. Sun, Y. L. Ji and J. F. Zhang, *J. Mater. Process. Technol.*, 306 (2022) 117641.
31. X. Q. Du, Y. W. Liu and Y. Chen, *Appl. Phys. A*, 127 (2021) 580.
32. X. T. Han, L. L. Ren, Y. Ma, X. Gong and H. X. Wang, *Carbon*, 197 (2022) 27.
33. H. Zheng, W. T. Liu, S. M. He, R. Wang, J. C. Zhu, X. D. Guo, N. J. Liu, R. B. Guo and Z. L. Mo, *Colloids Surf., A*, 648 (2022) 129152.
34. G. Q. Qiao, S. C. Wang, X. H. Wang, X. Y. Chen, X. Z. Wang and H. Z. Cui, *ChemPhysMater*, 1 (2022) 119.
35. M. Molaei, A. F. Alhosseini, M. Nouri, P. Mahmoodi and A. Nourian, *Ceram. Int.*, 48 (2022) 21005.
36. Y. P. Tang, Y. K. Cai, L. Wang, X. C. Luo, B. Wang, Q. H. Song and Z. Q. Liu, *Opt. Laser Technol.*, 153 (2022) 108190.
37. M. C. Wang, W. W. Wang, S. Q. Li, H. L. Liu, X. T. Fan and Z. Wang, *Prog. Org. Coat.*, 171 (2022) 107043.

© 2022 The Authors. Published by ESG ([www.electrochemsci.org](http://www.electrochemsci.org)). This article is an open access article distributed under the terms and conditions of the Creative Commons Attribution license (<http://creativecommons.org/licenses/by/4.0/>).